Rev. Adv. Mater. Sci. 55 (2018) 12-20

MAGNETIC SiO_2-Fe_3O_4 NANOCOMPOSITES AS CARRIERS OF IBUPROFEN FOR CONTROLLED RELEASE APPLICATIONS

M. González-Hurtado[1,2], J. A. Marins[3], B. Guenther Soares[4], J. Rieumont Briones[5], A. Rodríguez Rodríguez[2] and E. Ortiz-Islas[6]

[1]Institute of Materials Science and Technology, Polymer Laboratory,University of Havana, 10400 Havana City, Cuba
[2]Center for Research in Applied Science and Advanced Technology, IPN, Legaría 694, 11500 México City, México
[3]Institute of Physics of Nice, University Côte d'Azur, Parc Valrose, Nice 06100, France
[4]Laboratory of Polymer Blends and Composites Macromolecules Conductors, Institute of the Federal University of Rio de Janeiro,Av. Pedro Calmon 550, 21941-901 Rio de Janeiro, Brazil
[5]Department of Physical Chemistry, Faculty of Chemistry, University of Havana, 10600 Havana City, Cuba
[6]Nanotechnology Laboratory, National Institute of Neurology and Neurosurgery, Insurgentes Sur 3877, La Fama, 14269 México City, México

Received: June 24, 2018

Abstract. In the present paper, we report the preparation and characterization of magnetic silica nanostructured materials that were used as ibuprofen drug molecule carriers. This work was aimed at obtaining drug release systems sensitive to a magnetic field to be directed to target sites. The preparation of the silica nanostructured materials started with the synthesis of magnetite (Fe_3O_4) nanoparticles that were added subsequently during the hydrolysis and condensation of tetraethyl-orthosilicate (TEOS) to obtain SiO_2-Fe_3O_4 nanocomposites. The ibuprofen molecules were added simultaneously with magnetite nanoparticles. The *in vitro* ibuprofen release profiles were analyzed, showing a typical controlled release for all materials studied. The nanocomposites were characterized by Fourier transform infrared spectroscopy (FTIR), X-ray diffraction (XRD), scanning microscopy (SEM), thermogravimetric analysis (TGA), N_2 adsorption-desorption isotherms; magnetic studies were also performed. The obtained materials showed low superparamagnetic values, and saturation behavior was also observed. It was demonstrated that ibuprofen does not affect the magnetic behavior of magnetite, indicating its possible use in medical applications.

1. INTRODUCTION

Finding new methods for the encapsulation of drugs and controlling their delivery provides the means to achieve enhanced drug solubility and their accurate targeting, preventing premature drug degradation, permeate barriers, reduced dosage, and avoiding side effects [1-4]. At the present, drug delivery systems using nanomaterials as drug carriers have been widely reported [5-7]. Physicochemical properties of nano-carriers such as large surface areas, charge, hydrophobicity, shape, and rigidity are suitable to achieve an appropriate drug loading, drug release, and uptake nanomaterials within the body. Beside a wide range of drugs, small molecules, peptides, proteins, nucleic acids, and living cells have been incorporated also into nano-carriers [8,9].

There are several reported methods to encapsulate therapeutic agents that include both organic and inorganic materials and to obtain different shapes and structures such as nanoparticles, micro-nanospheres, nanotubes, and nanofibers, among others [2,9,10-12]. The application of an external

Corresponding author: E. Ortiz-Islas, e-mail: emma170@hotmail.com

stimulus to nano-carriers (such as temperature, pH, light, magnetic field, etc.) can control the drug concentration required at a specific site and at the same time can reduce side effects [13-16]. In particular, magnetic micro and nano particles might be ideal candidates for controlled drug release applications because they can be guided to the desired site by an external magnetic field application [15,17,18]. Because of its specific properties, such as superior magnetic properties, nontoxicity, small size, etc., Fe_3O_4 (magnetite) has been employed as a contrast agent to improve the signal intensity of magnetic resonance imaging (MRI). However, its application as vehicle of drugs is limited due to its agglomeration that correlates with nanoscale sizes, its large specific surface area, and the strong interaction of magnetic dipoles among particles [19,20]. To overcome these disadvantages, Fe_3O_4 magnetic nanoparticles have been modified or combined with organic or inorganic compounds such as polymers, metal, metal oxides, silica, and carbon materials [20-22], this has maintained their magnetic properties.

Because of its excellent properties such as high surface-to-volume ratio, high biocompatibility and biodegradability, easy functionalization, controllable porosity, and low cytotoxicity, silica-coated magnetic nanoparticles have become increasingly important for medical applications [23-25]. Silica is an ideal material to modify Fe_3O_4 nanoparticles because it can weaken the interaction of the magnetic dipoles among Fe_3O_4 nanoparticles to effectively overcome aggregation of the nanoparticles. The silanol groups on the surfaces of the silica coatings can improve the dispersity of nanoparticles. In addition, the silanol groups on the silica surfaces allow further modifications with various functional groups. Furthermore, it has been demonstrated that silica nanoparticles are biocompatible and chemically stable. Lately, silanol groups on the surfaces of silica could be used as coupling agents to facilitate drug loading and sustained release of drugs. Thus, the combined resultant SiO_2-Fe_3O_4 nanoparticles will have the magnetic properties of magnetite and the surface properties of silica.

A wide variety of drugs can be hosted in magnetic silica nanoparticles and the application of a magnetic field allows their delivery at the required site [25-30]. The use of combined silica-magnetite has been reported as a carrier of a water-insoluble immunosuppressive drug molecule (MPA: mycophenolic acid) [31], in gene delivery [32], for magnetic resonance imagen uses, and principally for anticancer drug delivery applications. Delivery of chemotherapeutic agents to specific target sites with a minimum of side effects is a major challenge for chemotherapy [33,34]. For example, targeting therapeutic agents to known tumor sites could substantially reduce toxicity through localization away from sensitive organs and through total dose reduction. Thus, magnetic silica is a good choice to use magnetic mesoporous silica (MMS) nanoparticles as a platform for chemotherapy.

In this paper, the preparation of silica nanoparticles by sol-gel method combined with magnetite nanoparticles is reported. The purpose is to obtain drug release carriers sensitive to magnetic fields. Ibuprofen was used as model drug and it was added during synthesis of the silica-Fe nanocomposites. It was proven that the drug does not vary the magnetic properties of magnetite; this property will enable using these systems for the release of drugs at specific sites.

2. EXPERIMENTAL

2.1. Chemical substances

Ferric chloride (Merck, 99%), hydrochloric acid, (Merck, 37%), sodium sulfite, (PANREAC, 96%), ammonium hydroxide, (PANREAC, 25%), ethanol (Fluka), Tetraethoxysilane (TEOS) (analytical grade, Aldrich), ibuprofen sodium salt (IBU) (Aldrich, 98%). All reagents were used as received.

2.2. Methods

Several SiO_2-magnetite (SiO_2-Mag) and SiO_2-magnetite-ibuprofen (SiO_2-Mag-IBU) samples were prepared using the sol-gel procedure and varying the TEOS:water molar ratio from 1:8, 1:16, and 1:24, respectively. The molar amounts used to prepare each sample are given in Table 1.

2.2.1. Sample synthesis

Magnetite nanoparticles (Mag). The magnetite particles were prepared following the method reported by Qu Shengchun [35] as follows:
20 mL of deionized water and 13.3 mL of 1.0 M sodium sulfite were added to 20 mL of 2.0 M ferric chloride. After, the formed iron complex was placed in a 1.5 M ammonium hydroxide solution and kept under ultrasonic agitation for 30 minutes. Next, the resulting nanoparticles were washed with distilled water until complete removal of the ammonium hydroxide. Finally, magnetite was placed in ethanol to obtain a magnetite-ethanol suspension at 10% weight.

Table 1. Experimental amounts of chemical substances used to prepare different magnetic silica samples. The amounts were adjusted to obtain 5 g of SiO_2.

Samples	TEOS [a](mol)	H_2O(mol)	Ethanol(mol)	IBU [b](mg)	Fe_3O_4(wt.%)
SiO_2 (1:8)	0.083	0.66	0.66	-	-
SiO_2 (1:16)	0.083	1.32	0.66	-	-
SiO_2 (1:24)	0.083	1.98	0.66	-	-
SiO_2-Mag (1:8)	0.083	0.66	0.66	-	7
SiO_2-Mag (1:16)	0.083	1.32	0.66	-	7
SiO_2-Mag (1:24)	0.083	1.98	0.66	-	7
SiO_2-Mag-IBU (1:8)	0.083	0.66	0.66	500	7
SiO_2-Mag-IBU (1:16)	0.083	1.32	0.66	500	7
SiO_2-Mag-IBU (1:24)	0.083	1.98	0.66	500	7

[a] Tetraethoxysilane, [b] ibuprofen

SiO_2-magnetite (SiO_2-Mag). The synthesis of each Fe_3O_4-SiO_2 sample was performed using the following procedure: the adequate amount of water, ethanol, and magnetite suspension were mixed and stirred at room temperature. Then, the TEOS amount was added by slow dripping in 4 h. Afterwards, the solution was maintained under mechanic stirring at room temperature for 24 h. Subsequently, the water and ethanol were removed using vacuum. Later, the sample was dried with vacuum during one week.

SiO_2-Mag-ibuprofen (SiO_2-Mag-IBU). As a first stage, the drug was mixed with water, ethanol, and magnetite suspension using mechanical stirring. Next, the TEOS amount was slowly added. Afterwards, the medium was maintained under stirring at room temperature for 24 h. Finally, the samples were dried under vacuum for one week.

2.2.2. Samples characterization

Fourier transformed infrared spectroscopy (FTIR). Each sample (~5 mg) was mixed with KBr (~95 mg); ground and compressed to form a translucent wafer. The wafer was placed in a FTIR-THERMO NICOLET Nexus-670 spectrophotometer to collect the FTIR spectrum in the wavenumber region between 500 and 4000 cm^{-1}.

Thermogravimetric analysis (TGA). The samples were heated from 30 to 800 °C at a rate of 20 °C/min applying a nitrogen flux. The TGA profiles were recorded using a TA thermal analyzer Q50 Apparatus.

N_2 adsorption-desorption. The specific surface area, average pore diameter, and pore volume were determined from the nitrogen adsorption-desorption isotherms. The samples were previously activated at 100 °C with vacuum during 16 h. The nitrogen gas adsorption-desorption was carried out at 77.3K using a Micromeritics (ASAP 2405 N) equipment. The specific surface areas was determined using the Brunauer-Emmet-Teller (BET) method, while the average pore size and pore volume were determined from the desorption isotherms using the Barret-Joyner-Halenda (BJH) method.

X-Ray diffraction (XRD). The X-ray diffraction patterns were obtained using a Rigaku diffractometer (Miniflex model) containing a Bragg-Brentano geometry and CuKα radiation of 1.5408 Å, monochromator operated at 35 kV and 25 mA. The samples were scanned in the 2θ = 2-70° range, with a step time of 2 s and a step size of 0.05°.

Scanning electron microscopy (SEM). The microphotographs were taken in a SEM JEOL-5600 LV electronic microscope at 20 kV. Samples were coated with a gold layer of approximately 20 nm thickness using an EMS 550 sputter coating.

Magnetic analysis. The magnetic properties of the samples were evaluated using an MPMS-3 magnetometer from Quantum Design. The magnetization curves versus applied magnetic field were recorded in the -7 to 7 Tesla range at 1.8 and 300K.

2.2.3. In vitro drug release tests

In vitro release tests were performed at laboratory scale, according to USP XXVII recommendations. Each sample was suspended in 150 mL of a 0.1 M HCl/2 M Na_3PO_4 solution (volume:volume ratio of 3:1 and pH = 6.8). The dissolution medium was kept under stirring at 100 rpm. At appropriate time intervals, 3 mL of each sample were removed for their spectrophotometric measurement at λ = 265 nm in the UV region. All the experiments were carried out at 37 °C ± 0.20 °C. The released ibuprofen amount

Table 2. Yield and encapsulation efficiency (*E.E*) values.

Samples	Yield(%)	*E.E*(%)
SiO_2-Mag-IBU (1:8)	70. 5	55. 6
SiO_2-Mag-IBU (1:16)	82. 3	66. 4
SiO_2-Mag-IBU (1:24)	80. 1	60. 2

was determined with a calibration curve that followed the C= 0.1511A + 0.1134 linear regression. All samples were studied in duplicate.

2.2.4. Encapsulation efficiency (*E.E*) determination

The amount of ibuprofen (IBU) loaded in each sample was estimated directly by dissolving 5 mg of SiO_2-Mag-IBU sample in 1 mL of 0.1 M phosphate-buffered saline (PBS) at room temperature. Thereafter, each solution was measured at 265 nm to determine the amount of IBU. The percentage of encapsulation efficiency (*E.E* %) was calculated employing the following equation, Eq. (1) :

$$E.E(\%) = \frac{\text{Experimental encapsulation ratio}}{\text{Theoretical encapsulation ratio}} \times 100. \quad (1)$$

The yield (*Y*,%) was calculated using the following equation (2):

$$Y(\%) = \frac{mp}{mp.a + mref} \times 100, \quad (2)$$

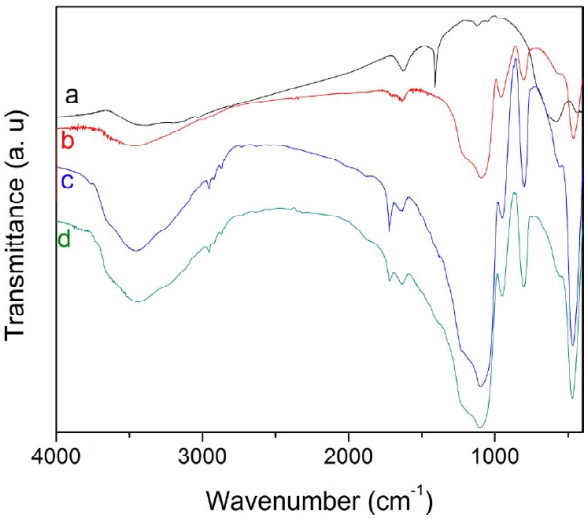

Fig. 1. Infrared spectra of (a) magnetite, (b) SiO_2, (c) SiO_2-Mag (1:8) and (d) SiO_2-Mag (1:16) samples.

where: *mp* is the total amount of each obtained sample; *mp.a* is the amount of IBU; *mref* is the amount of SiO_2 without IBU.

3. RESULTS AND DISCUSSION

3.1. Yield (*y*) and encapsulation efficiency (*E.E*)

Table 2 shows the *Y* (%) and *E.E* (%) values for the different samples. It is possible to determine that the best *Y* (%) and *E.E* (%) were obtained for the SiO_2-Mag-IBU (1:16) sample. These results can be related to the synthesis parameters, which indicate that this is the ideal molar water-alkoxide rate.

3.2. Fourier transform infrared spectroscopy (FTIR)

Fig. 1 depicts the infrared spectra of magnetite, silica, and silica-magnetite samples prepared with different water concentrations. Magnetite spectrum shows a weak band around 3443 cm^{-1} that is due to the stretching vibration modes of -OH groups on the surface of the oxide. The band at 1629 cm^{-1} is attributed to the vibration modes of deformation of the H-O-H bonds from water molecules adsorbed on the hydrophilic surface of metal oxide. The peaks at 581 cm^{-1} and 425 cm^{-1} correspond to vibrations of Fe^{3+}/Fe^{2+}–O^{2-} of tetrahedral and octahedral sites, respectively, in the spinel structure of Fe_3O_4 [36]. The bands at 3057 and 1405 cm^{-1} may be attributed to vibrations of Fe-NO_2 due to residual ammonia even after several washings [37].

The silica spectrum shows its characteristic bands. The broad band at 3696-3156 cm^{-1} and the band at 1629 cm^{-1} identify physical adsorbed water. The band at 950 cm^{-1} is attributed to surface hydroxyl groups (Si–OH). The broad band at 1302-1005 cm^{-1} belongs to the skeletal Si–O–Si matrix. The bands at 800 and 455 cm^{-1} are due to the vibration and deformation of Si–O–Si bending modes. The small peaks at approximately 2960 cm^{-1} come from the residual alkoxide groups.

In the spectra of SiO_2-Mag samples, the bands that correspond to both silica and magnetite are seen; suggesting that magnetite did not change during the synthesis process.

Fig. 2 shows the IBU and IBU-silica-magnetite spectra. Ibuprofen is an organic compound with the chemical structure shown in Fig. 2e and its IUPAC name is: (RS)-2-(4-(2-methylpropyl) phenyl) propanoic acid. Ibuprofen contributes with some signals in the infrared spectrum as shown in Fig. 2a. The strong absorptions between 3108 and 2840 cm^{-1}

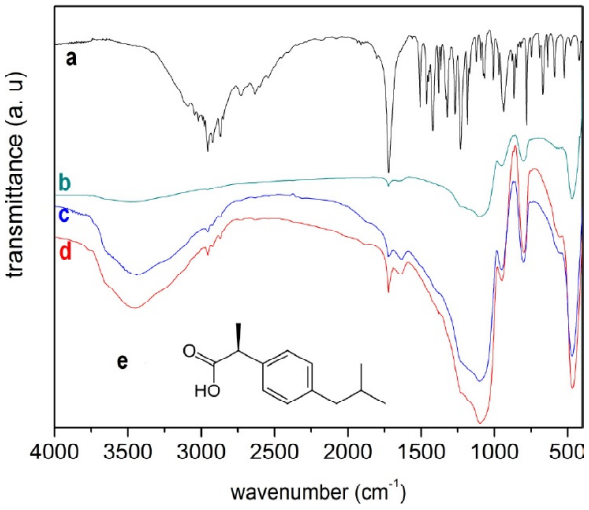

Fig. 2. Infrared spectra of (a) ibuprofen molecule, (b) SiO_2-Mag-IBU (1:24), (c) SiO_2-Mag-IBU (1:16), (d) SiO_2-Mag-IBU (1:8) and (e) Chemical structure of the ibuprofen molecule.

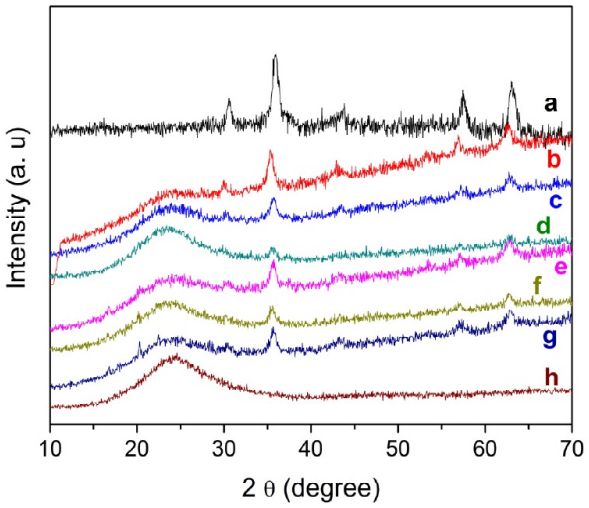

Fig. 3. X-ray diffraction patterns (XRD) of (a) magnetite, (b) SiO_2-Mag (1:8), (c) SiO_2-Mag (1:16), (d) SiO_2-Mag (1:24), (e) SiO_2-Mag-IBU (1:8), (f) SiO_2-Mag-IBU (1:16), (g) SiO_2-Mag-IBU (1:24) and (h) SiO_2 samples.

correspond to C-H stretch vibrations from its long carbon chain. The prominent C=O stretch vibrations of the carboxylic acid moiety of IBU was located at 1710 cm^{-1}. The bands at 1502 and 781 cm^{-1} are attributed to C-C and C-H vibrations, respectively. The spectra of the samples containing IBU showed the most important bands of the IBU: C=O at 1725 cm^{-1}, C-H between 3011 and 2789 cm^{-1}. The signals corresponding to magnetite are seen also, but the band at 1405 cm^{-1} disappeared, indicating that NO_2 species were not formed. It was also possible to identify the signals corresponding to silica.

3.3. X-Ray diffraction (XRD)

Fig. 3 displays the X-ray diffraction patterns of Fe_3O_4 (Mag), silica, silica-Mag, and silica-Mag-IBU samples. The magnetite's diffractogram exhibits six different diffractions at 2q degrees of 16.12 (1 1 1), 30.52 (2 2 0), 35.94 (3 1 1), 43.70 (4 0 0), 57.63 (5 1 1), and 63.21 (4 4 0) that are classified as the cubic inverse spinal structure of magnetite. The X-ray analysis also indicates the absence of other types of iron oxide in the synthetized product. The diffractogram corresponding to silica's reference only shows a broad peak that is characteristic of an amorphous silica material. In all diffractograms of the SiO_2-Mag samples, the diffraction peaks corresponding to magnetite were observed, and they are in the same position as those of pure magnetite, indicating a successful load of magnetite on silica. In a similar way, in the SiO_2-Mag-IBU diffraction patterns, the diffractions corresponding to magnetite are also seen.

3.4. Thermogravimetric analysis (TGA)

Fig. 4 shows the thermogram of SiO_2-Mag-IBU (1:16) sample. It is possible to identify a first weight loss between the initial temperature of treatment and 180°C, which was of about 16%. This loss is derived from the initial water evaporation and from IBU elimination (melting point 75-78 C) as a 10% weight of IBU was loaded on silica. A second weight loss is observed between 130 and 455 °C, corresponding to total evaporation of adsorbed water molecules and elimination of residual organic material (precursor compounds) with a loss of 2%. The third weight loss is found between 455 and 600 °C with a 7%,

Table 3. Weight loss at different temperature intervales of SiO_2-Mag-IBU samples.

Sample	Weight Loss (%)		
	25-134 °C	134-395 °C	395-582 °C
SiO_2-Mag-IBU (1:8)	18	4	7
SiO_2-Mag-IBU (1:16)	16	2	7
SiO_2-Mag-IBU (1:24)	14	4	7

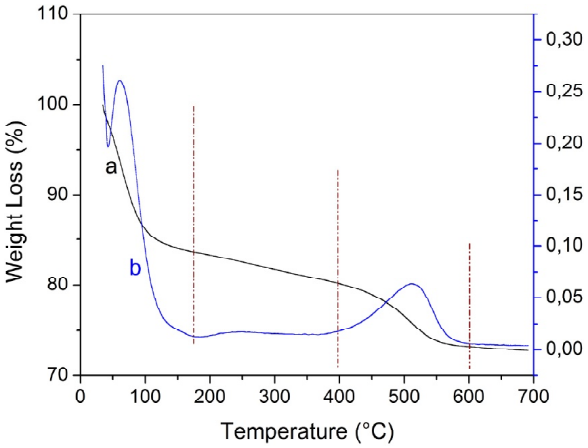

Fig. 4. (a) Thermogram and (b) thermogram derived of the SiO_2-Mag-IBU (1:16) sample**.**

which is attributed to structural changes of magnetite as this percentage corresponds to the magnetite loaded on silica. It has been reported that magnetite oxidation can occur around 600 °C [38]. The other thermograms are similar to that described previously (not shown). Table 3 depicts the weight loss at different temperature ranges for all samples. In general, the weight loss percentage for each temperature interval is similar for each sample.

3.5. Nitrogen adsorption-desorption measurements

Table 4 depicts the surface area, pore diameter, and pore volume values of all samples. Silica samples prepared with different water concentrations have the highest surface area values. In these samples, the surface area increased as the water quantity increased. In the same sense, the size and pore volume increased. In contrast, the surface area decreased in samples containing IBU. This is because the IBU molecules occupied part of the total surface of silica. According to IUPAC's classification, the pore sizes for silica samples are meso-pores, whereas the pores of the samples containing the drug are macro-pores. However, the pore volume decreases in samples containing the drug because that volume is occupied by the drug molecules.

3.6. Scanning electron microscopy (SEM)

The SEM figures of the different nanostructured materials are shown in Fig. 5. The main features indicate a heterogeneous morphology with clusters of different sizes and a rough surface. There is no sharp difference in morphology among the composites. However, it is possible to observe very well defined particles, when the water molar ratio is increased.

3.7. Magnetization studies

Table 5 provides the magnetic properties for the different samples containing IBU. The saturation magnetization (*Ms*) and coercivity (*Hc*) values were obtained at 300K from the experimental hysteresis-curve (Fig. 6). The concentration of IBU bound to the surface of the nanoparticles (nanostructured materials) does not affect the value of the coercive field. *Hc* values at different temperatures suggest a typical behavior of superparamagnetic materials [39] as expected for particles with nanometric sizes. Moreover, the saturation magnetization at 300K in each sample decreased about 0.4 emu/g compared to the values obtained at 1.8K, ensuring that there are no other processes that may affect magnetic saturation.

Fig. 6 shows the hysteresis curves for SiO_2-Mag-IBU samples at 300K. Note that saturation is reached rapidly from 0.5 T to 1.5 T, guaranteeing the maximum particle orientation. The SiO_2-Mag-IBU (1:16) shows a lower saturation and, therefore, a low magnetization value. If the samples were used in clinical applications, these materials allow us to

Table 4. Surface properties of silica and silica-Mag-IBU samples.

Sample	S_{BET} (m^2/g)[a]	P_D (nm)[b]	P_V (cc/g)[c]
SiO_2 (1:8)	560	3.1	0.435
SiO_2 (1:16)	674	7.4	1.25
SiO_2 (1:24)	957	4.2	1.0138
SiO_2-Mag-IBU (1:8)	354	41.8	0.037
SiO_2-Mag-IBU (1:16)	23	33.9	0.20
SiO_2-Mag-IBU (1:24)	81	26.1	0.0053

[a] Surface area obtained using the BET equation, [b] the pore diameter, and [c] pore volume.

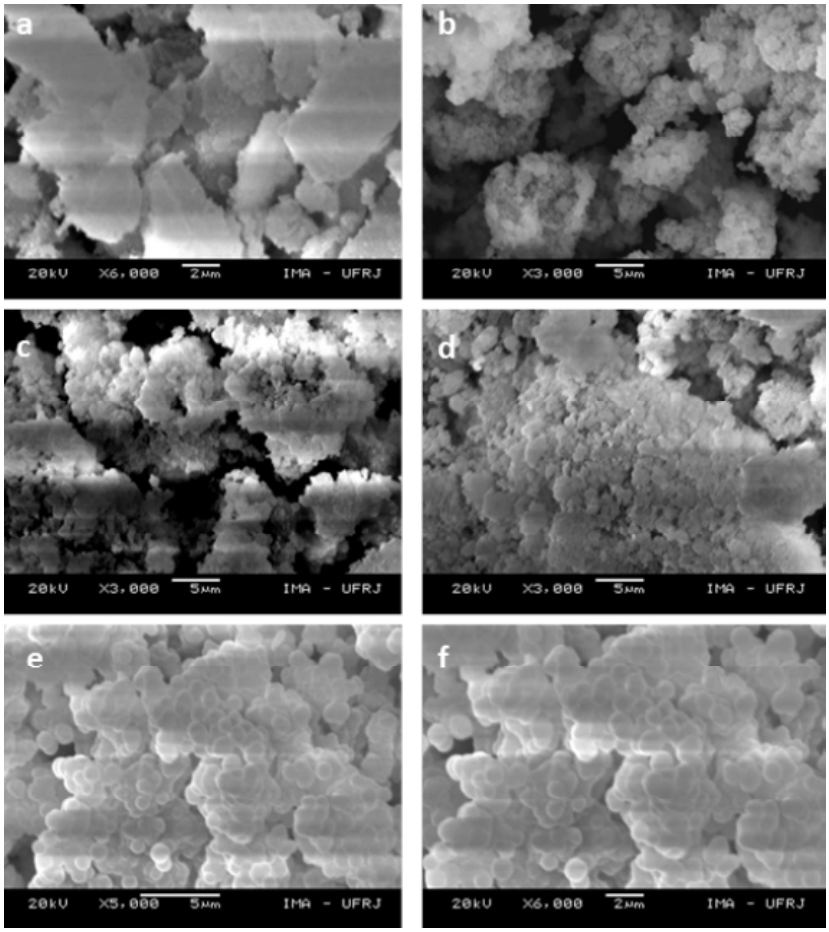

Fig. 5. SEM images of (a, b) SiO_2 at X6000 and X3000 respectively, (c, d) SiO_2-Mag both at X3000 and (e, f) SiO_2-Mag-IBU at X3000 and X6000 respectively.

protect the patient by applying low magnetic fields without affecting the magnetic nanoparticles performance. It was demonstrated that ibuprofen did not affect the magnetic field behavior of magnetite.

Table 5. Magnetic values obtained at 1.8 and 300K of SiO_2-Mag-IBU samples.

Sample	$Ms_{(emu/g)}$ [a]	$H_{c(Oe)}$ [b]
SiO_2-Mag-IBU (1:8)		
1.8K	4.17	420
300K	3.33	23
SiO_2-Mag-IBU (1:16)		
1.8K	2.38	300
300K	1.94	20
SiO_2-Mag-IBU (1:24)		
1.8K	2.80	367
300K	2.37	26

[a] Saturation magnetization, [b] Coercive Force

3.8. *In vitro* ibuprofen release profiles

Fig. 7 depicts the IBU release profiles of the SiO_2-Mag-IBU samples. All samples presented an initial burst and a portion of the IBU was trapped inside these materials. In all cases, a typical controlled release behavior is shown. The released amount corresponds to the IBU molecules located on the silica surface. SiO_2-Mag-IBU (1:16) sample showed the best release profile and the best encapsulation efficiency (66 %).

Table 6 provides the kinetic parameters of the experimental values adjusted to different mathematical models. The kinetic study shows that the ibuprofen release was controlled by a Fick diffusion mechanism through the matrix (r^2> 0.97) for all samples. Furthermore, part of the IBU stays trapped within the matrix. It is to be observed from Table 4 that the BET surface and pore volumes are quite low for these stiff materials, which could be responsible for the observed burst effect and entrapment [40].

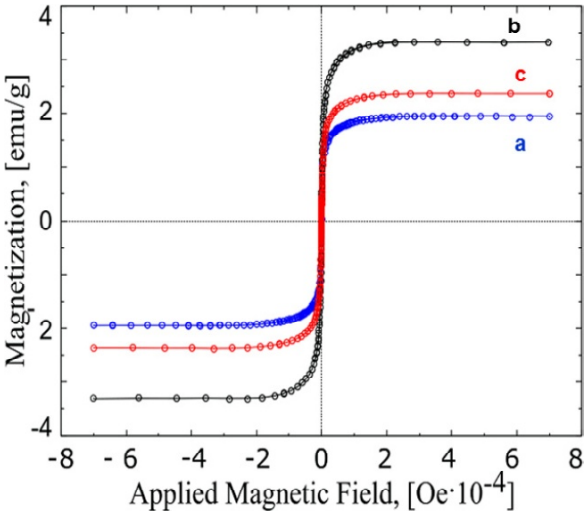

Fig. 6. Hysteresis-curves obtaind at 300K of SiO_2-Mag-IBU samples prepared with molar ratios of a) 1:16, b) 1:8, c) 1:24, respectively.

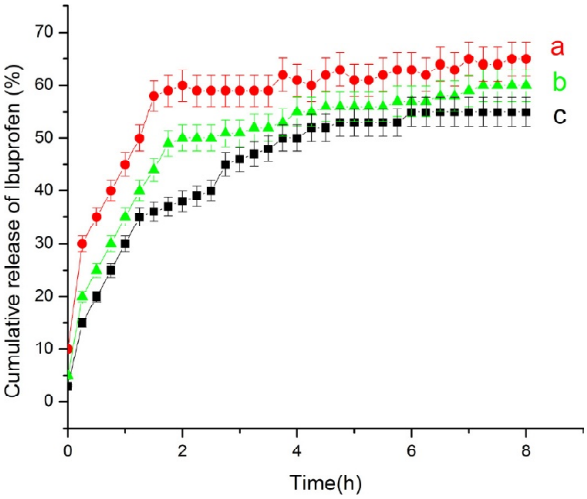

Fig. 7. Cumulative release profiles of ibuprofen related to encapsulation efficiency (E.E) of a) SiO_2-Mag-IBU (1:24), b) SiO_2-Mag-IBU (1:16) and c) SiO_2-Mag-IBU (1:8) samples.

4. CONCLUSIONS

Magnetic silica nanostructured materials were obtained by the combination of magnetite and silica. Magnetite was the only phase present in all samples. All synthesized materials were mesoporous. Ibuprofen molecules were well stabilized into the magnetic silica nanostructured materials and they were released in two different steps. The drug release mechanism was controlled by a Fick diffusion of ibuprofen through pores of silica. It was demonstrated that ibuprofen did not affect the magnetic field behavior of magnetite. Low saturation magnetization values were obtained indicating an acceptable use of these nanostructured materials in medical applications. Low magnetic fields will be necessary to avoid affecting the magnetic performance of the nanostructured materials.

ACKNOWLEDGEMENTS

Dr. Mayra González Hurtado is grateful to TWAS and CONACYT (2015-2016) for the award of a Postdoctoral Fellowship and the financial support. We gratefully acknowledge the support of the Centro de Investigación en Ciencia Aplicada y Tecnología de Avanzada, IPN, México City, México.

REFERENCES

[1] E. Blanco, H. Shen and M. Ferrari // *Nat. Biotechnol*. **33** (2015) 941.
[2] R. Fernandes and D.H. Gracias // *Adv. Drug. Deliv. Rev*. **64** (2012) 1579.
[3] V. Sharma, S. Anandhakumar and M. Sasidharan // *Mater. Sci. Eng. C Mater. Biol. Appl.* **56** (2015) 393.
[4] U. Wais, A.W. Jackson, T. He and H. Zhang // *Nanoscale* **8** (2015) 1746.
[5] X.J. Cai and Y.Y. Xu // *Cytotechnology* **63** (2011) 319.
[6] N. Habibi, N. Kamaly, A. Memic and H. Shafiee // *Nano. Today* **11** (2016) 41.
[7] M. Palombo, M. Deshmukh, D. Myers, J. Gao, Z. Szekely and P.J. Sinko // *Annu. Rev. Pharmacol. Toxicol.* **54** (2014) 581.
[8] C. Iancu, I.R. Ilie, C.E. Georgescu, R. Ilie, A.R. Biris, T. Mocan, L.C. Mocan, F. Zaharie, D. Todea-Iancu, S. Susman, D. Ciuca and A.S. Biris // *Partcul. Sci. Technol.* **27** (2009) 5624.

Table 6. Correlation coefficients (r) for linear relationship of the proposed combined kinetics of SiO_2-Mag-IBU samples.

Sample	Zero Order r^2	First Order r^2	Fickr^2	Hixson Crowell r^2
SiO_2-Mag-IBU (1:8)	0.92	0.78	0.99	0.84
SiO_2-Mag-IBU (1:16)	0.90	0.74	0.98	0.80
SiO_2-Mag-IBU (1:24)	0.95	0.82	0.99	0.87

[9] M. Malmsten // *Curr. Opin. Colloid. Int.* **18** (2013) 468.
[10] R. Jayakumar, D. Menon, K. Manzoor, S.V. Nair and H. Tamura // *Carbohydr. Polym.* **82** (2010) 227.
[11] N. Kameta // *J. Incl. Phenom. Macrocycl. Chem*. **79** (2014) 1.
[12] C. Sanchez, P. Belleville, M. Popalld and L. Nicole // *Chem. Soc. Rev*. **40** (2011) 696.
[13] M. Karimi, P.S. Zangabad, A. Ghasemi and M.R. Hamblin, In: *Smart External Stimulus-Responsive Nanocarriers for Drug and Gene Delivery*, ed. by Morgan &Claypool Publishers (2015).
[14] M. Nakayama, T. Okano, T. Miyazaki, F. Kohori, K. Sakai and M. Yokoyama // *J. Control. Release.* **115** (2006) 46.
[15] H. Shagholani, S.M. Ghoreishi and M. Mousazadeh // *ýInt. J. Biol. Macromolec.* **78** (2015) 130.
[16] K.S. Soppimath, T.M. Aminabhavi, A.M. Dave, S.G. Kumbar and W.E. Rudzinski // *Drug. Dev. Ind. Pharm*. **28** (2002) 957.
[17] S. Guo, D. Li, L. Zhang, J. Li and E. Wang// *Biomaterials* **30** (2009) 1881.
[18] C.W. Zhang, C.C. Zeng and Y. Xu // *NANO: Brief Reports and Reviews* **9** (2014) 1.
[19] M. Ahmed and M. Douek // *Bio. Med. Research. International* **2013** (2013) 1.
[20] J. Xu, F. Zhang, J. Sun, J. Sheng, F. Wang and M. Sun // *Molecules* **19** (2014) 21506.
[21] F. Chen, L. Zhang, Q. Chen, Y. Zhang and Z. Zhang // *Chem. Commun*. **46** (2010) 8633.
[22] E.V. Escobar, C.A. Martínez, C.A. Rodríguez, J.S. Castro, M.A. Quevedo and P.E. García-Casillas // *J. Alloys. Compd.* **536S** (2012) S441.
[23] S. Abramson, W. Safraou, B. Malezieux, V. Dupuis, S. Borensztajn, E. Briot and A. Bée // *J. Colloid. Interface. Sci*. **364** (2011) 324.
[24] T. Liu, L. Liu, J. Liu, S. Liu and S.Z. Qiao // *Front. Chem. Sci. Eng*. **8** (2014) 114.
[25] K. Viswanathan // *Colloids and Surfaces A: Physicochem. Eng. Aspects.* **386** (2011) 11.
[26] B. Chang, J. Guo, C. Liu, J. Qian and W. Yang // *J. Mater. Chem*. **20** (2010) 9941.
[27] S. Hu, T. Liu, H. Huang, D. Liu and S. Chen // *Langmuir* **24** (2008) 239.
[28] J.E. Lee, N. Lee, H. Kim, J. Kim, S.H. Choi, J.H. Kim, T. Kim, I.C. Song, S.P. Park, W.K. Moon and T. Hyeon // *J. Am. Chem. Soc.* **132** (2010) 552
[29] K.C. Souza, J.D. Ardisson and E.M.B. Sousa // *J. Mater. Sci: Mater. Med.* **20** (2009) 507.
[30] C. Tao and Y. Zhu // *Dalton. Trans*. **43** (2014) 15482.
[31] J. Hwang, E. Lee, J. Kim, Y. Seo, K.H. Lee, J.W. Hong, A.A. Gilad, H. Park and J. Choi // *Colloids Sur. B* **142** (2016) 290.
[32] O. Mykhaylyk, T. Sobisch, I. Almstätter, Y. Sanchez-Antequera, S. Brandt, M. Anton, M. Döblinger, D. Eberbeck, M. Settles, R. Braren, D. Lerche and C. Plank // *Pharm. Res.* **29** (2012) 1344.
[33] G. Yang, H. Gong, T. Liu, X. Sun, L. Cheng and Z. Liu // *Biomaterials* **60** (2015) 62.
[34] Y. Zhou, Y. Zeng, S. Huang, Q. Xie, Y. Fu, L. Tan, M. Ma and S. Yao // *Sens. Actuators, B* **173** (2012) 433.
[35] S. Qu, H. Yang, D. Ren, S. Kan, G. Zou, D. Li and M. Li // *J. Colloid. Interface. Sci.* **215** (1999) 190.
[36] M. Khalkhali, K. Rostamizadeh, S. Sadighian, F. Khoeini and M. Naghibi // *Materials* **6** (2013) 184.
[37] M. Abboud, S. Youssef, J. Podlecki, R. Habchi, G. Germanos and A. Foucaran // *Mater. Sci. Semicond. Process* **39** (2015) 641.
[38] M. Khalkhali, K. Rostamizadeh, S. Sadighian, F. Khoeini, M. Naghibi and M. Hamidi // *J Pharm. Sci.* **23** (2015) 45.
[39] T. Neuberger, B. Schöpf, H. Hofmann, M. Hofmann and B. von Rechenberg // *J. Magn. Magn. Mater.* **293** (2005) 483.
[40] M.H. Shoaib, J. Tazeen, H.A. Merchant and R.I. Yousuf // *Pak. J. Pharm. Sci*. **19** (2006) 119.